Microporous and Mesoporous Materials 274 (2019) 347–355

Contents lists available at ScienceDirect

Microporous and Mesoporous Materials

journal homepage: www.elsevier.com/locate/micromeso

Fabrication and stability exploration of hollow fiber mordenite zeolite membranes for isopropanol/water mixture separation

Chuan Chen[a], Yuli Cheng[a], Li Peng[a], Chun Zhang[a], Zhengqi Wu[a], Xuehong Gu[a,*], Xiaoyu Wang[b], Sohail Murad[b]

[a] State Key Laboratory of Materials-Oriented Chemical Engineering, College of Chemistry and Chemical Engineering, Nanjing Tech University, 5 Xinmofan Road, Nanjing, 210009, PR China
[b] Department of Chemical and Biological Engineering, Illinois Institute of Technology, Chicago, IL, 60616, USA

ARTICLE INFO

Keywords:
Mordenite zeolite membrane
Pervaporation
Hollow fiber
Vapor permeation
Isopropanol dehydration

ABSTRACT

High performance mordenite zeolite membranes were fabricated on four-channel Al_2O_3 hollow fiber substrates for the first time by using ball-milled mordenite particles as seeds. It was found that the particle size of seed played a vital part in the growth of membrane layers. The mordenite particles with a size of approximately 300 nm via ball milling enabled the growth of zeolite to form a uniform and defect-free zeolite membrane. The as-fabricated membranes showed high performance for isopropanol (IPA)/water mixtures separation. For IPA/H_2O (90/10 wt%) mixture dehydration at 75 °C by pervaporation, the permeation flux of 1.43 kg m^{-2} h^{-1} and the separation selectivity of > 10000 were achieved. The influence of feed water content on the separation performance of mordenite membrane was studied in detail. In addition to good dehydration performance at a low feed water content, the mordenite zeolite membranes also demonstrated long time stable separation performance for high feed water content systems. Permporosimetry measurements and molecular simulations showed that, unlike NaA zeolite crystal, the adsorbate water affected the expansion/contraction of MOR zeolite crystal framework weakly. Our research shows that MOR zeolite membrane shows good potential for the industrial solvent dehydration applications.

1. Introduction

Membrane separation technology has received much attention for the separation and purification of organic solvents, especially for the azeotropes separation recently, due to the advantages of saving energy [1,2]. As one kind of inorganic membrane materials possessing the properties of chemical stability, hydrothermal stability and unique pore system, zeolite membranes demonstrate good potential in the organic solutions separation [3–11]. Hydrophilic NaA zeolite membranes have been already industrially applied in organic solvent dehydration in the past few years [12,13], showing high separation performance for ethanol (EtOH) dehydration by vapor permeation. However, the application of NaA zeolite membrane in IPA/H_2O mixtures separation by the method of vapor permeation has been limited, because of its poor separation performance when the water content of the feed is either low or high. Previous studies have shown that, the contractions of NaA zeolite crystals, which increase the sizes of the intercrystalline defects, and the finding that the water adsorbed at the defects of membrane at low loading of water cannot block the intercrystalline defects are the reasons for the poor dehydration performance when the water content in the feed is low [14,15]. Under water rich conditions, the degradation of the crystallinity of NaA due to its low Si/Al ratio makes NaA membranes unstable for the long time dehydration of organic solution at high feed water content [16].

Possessing the effective pore size of 0.26 × 0.57 nm^2 parallel to a-axis and 0.67 × 0.70 nm^2 parallel to c-axis, mordenite zeolite membrane has been thought to be a promising candidate for solvents dehydration because of its good hydrophilicity and the resulting structural stability originating from its relatively high Si/Al ratio of 5–10 [17–20]. In recent decades, several studies have been carried out to synthesize mordenite zeolite membrane and optimize its structure. Without using organic template, Lin et al. [21] prepared mordenite membranes on the surface of α-Al_2O_3 tubular substrates with in-situ hydrothermal synthesis method, which revealed a permeation flux of 0.1 kg m^{-2}·h^{-1} with the separation selectivity of 3360 for IPA/H_2O (90/10 wt%) mixtures dehydration at the temperature of 75 °C. Li et al. [17] successfully fabricated c-oriented mordenite membranes. For the separation of IPA/H_2O in the same above mentioned condition, the permeation flux

* Corresponding author.
E-mail address: Xuehonggu@yahoo.com (X. Gu).

https://doi.org/10.1016/j.micromeso.2018.09.010
Received 23 May 2018; Received in revised form 7 September 2018; Accepted 10 September 2018
Available online 12 September 2018
1387-1811/

increased to 0.65 kg m^{-2} h^{-1} and the separation selectivity increased to 5000. To further improve flux of membrane, Navajas et al. [22] developed a post-synthesis alkali treatment method. After alkali treatment, the mordenite membranes showed improved separation performance: for EtOH/H_2O (90/10 wt%) mixture dehydration, the flux increased from 0.2 kg m^{-2} h^{-1} to 0.91 kg m^{-2} h^{-1} and the separation selectivity increased from 150 to 203. By adding F^- ions in the starting gel, Zhou et al. [23] fabricated mordenite membranes on mullite support, which possessed a high average permeation flux of 1.5 kg m^{-2} h^{-1} and an average selectivity of 1380 for EtOH/H_2O (90/10 wt%) mixture separation at 75 °C. Zhu et al. [24] adopted a microwave-assisted method to synthesize mordenite membranes, showing a high permeation flux of 1.10 kg m^{-2} h^{-1} and a separation selectivity as high as 7500 for EtOH/H_2O (90/10 wt%) system separation at 75 °C. Despite these developments, the separation performance of mordenite zeolite membrane still needs to be improved further for the practical application.

Four-channel ceramics hollow fiber substrates with thin substrate thickness can be expected to reduce transport resistance and improve the flux of membrane. The α-Al_2O_3 hollow fiber supported NaA zeolite membranes demonstrated a high permeation flux as high as of 12.8 kg m^{-2} h^{-1} [25] in procedure of EtOH/H_2O (90/10 wt%) mixture dehydration at 75 °C. Moreover, high mechanical strength and the high loading density of ceremic hollow fiber substrates are beneficial for industrialization of mordenite zeolite membranes.

In this paper, we gave a report of the successful preparation of mordenite membranes on four-channel ceramics hollow fiber substrates by secondary hydrothermal synthesis. The formation of defect-free mordenite zeolite layers was induced by using ball-milled submicron mordenite particles as seeds. The influence of mordenite seeds size on the quality of obtained zeolite membrane was studied in detail. The performance of the obtained mordenite zeolite membranes for IPA/H_2O mixture separation at different water content in the feed was investigated extensively. Permporosimetry studies and molecular simulation were carried out to study the influence of water adsorption on the MOR zeolite crystal unit cell size and the size of defects in the zeolite membrane, which show that the framework of MOR zeolite is relatively rigid and is less affected by the water adsorption compared with NaA zeolite.

2. Experiment section

2.1. Synthesis of mordenite zeolite membranes

Mordenite zeolite membranes were fabricated on the surface of homemade four-channel α-Al_2O_3 ceramics hollow fiber substrates by the secondary hydrothermal growth. The substrates had outer diameter of 4 mm with length of 70 mm, average pore size of 0.55 μm, porosity of 55–60%, respectively [25]. Firstly, the substrates were soaked in 0.5 wt % sodium hydroxide solution for 8 h, and then in deionized water for 30 min and dried at 70 °C in the oven for 8 h. Prior to hydrothermal synthesis, the support surface was coated with mordenite seed crystals by a simple dip-coating method. The composition of synthesis for mordenite seed crystals was 30 SiO_2: 1 Al_2O_3: 8.4 Na_2O: 900H_2O. The synthesis solution was achieved by dissolving $NaAlO_2$ (50–56 wt% Al_2O_3, Sigma-Aldrich, America), colloidal silica (Ludox SM-30, Sigma-Aldrich, America), NaOH (99 wt%, Sinopharm Chemical Reagent Co., Ltd, China) in distilled (D.I.) water at 20–25 °C under stirring for 6 h. The synthesis solution was crystallized at 170 °C for 48 h. The resultant mordenite zeolite particles with an average size of about 4 μm were ball-milled for several hours to get smaller zeolite seeds. The coating solution was prepared by dispersing 0.2 g ball-milled seeds in 20 g D.I. water, and the substrates were immersed vertically into 1 wt% seed suspensions for 10 s. After drying at 70 °C for 8 h, the seeded supports were used for synthesis of mordenite membrane. For the mordenite membrane synthesis, the precursor with the molar composition of 15 SiO_2: 1 Al_2O_3: 3 Na_2O: 750H_2O: 1.2 K_2O: 1.5 NH_4F was prepared by dissolving $NaAlO_2$, NaOH, KOH (85 wt%, Sinopharm Chemical Reagent Co., Ltd, China), NH_4F (98 wt%, Sinopharm Chemical Reagent Co., Ltd, China) and colloidal silica in D.I. water under stirring for 6 h at 20–25 °C. Then, the hydrothermal synthesis was performed at 170 °C for 16 h. The as-fabricated membranes were washed repeatedly by D.I. water and dried in an oven for more than 4 h before dehydration tests.

2.2. Characterization

The morphologies of mordenite seeds and mordenite membranes were observed by FE-SEM (S-4800, Hitachi). Mordenite seeds and mordenite membranes phases were verified by XRD, (MiniFlex 600, Rigaku) and the 2 θ range of Cu-Kα radiation source is 5–50°. The volume size distributions of mordenite particles were analyzed by a particle size analyzer (NPA152-31A Zetatrac, Microtrac Inc.).

2.3. Pervaporation (PV) and vapor permeation (VP) tests

Pervaporation and vapor permeation for organic mixture separation were conducted and the PV and VP facility were described schematically in our previous work [14,26]. The feed side and permeate side was kept at atmospheric pressure, and a pressure of < 200 Pa, respectively. Gas chromatograph (GC-2014, Shimadzu) equipped with a TCD was used to analyze water mass concentration. The membrane's PV and VP performance results are determined by separation factor (α) and the permeation flux [Q/(kg·m^{-2}·h^{-1})]. The separation factor (α) and the permeation flux [Q/(kg·m^{-2}·h^{-1})] are defined as

$$\alpha = \frac{Y_{water}/Y_{isopropanol}}{X_{water}/X_{isopropanol}} \quad (1)$$

$$Q = \frac{M}{A \cdot t} \quad (2)$$

where X and Y are the mass concentration of components in the feed and permeate, respectively; M (kg) is the weight of the permeate; A (m^2) is the effective area of zeolite membrane; and t (h) is the collecting time.

2.4. Permporosimetry measurement experiments

The permporosimetry test system was described in detail in our previous paper [27]. The quality of zeolite membranes was assessed by characterizing helium (He) permeability through the membranes. Before conducting the tests, the mordenite membranes inserted in the membrane module were dried at 100 °C in a flowing He stream for 8 h to remove adsorbate water in the pores of zeolite and defects. Subsequently, the operation temperature was reduced to 40 °C during the test. The differential pressure between feed and permeate was maintained at 0.1 MPa. The feed stream included two He streams: one was a pure He stream; the other was He stream saturated with adsorbate vapor, which was produced by loading water or alcohols (methanol, ethanol, isopropanol) with high purity through paking few CaO powders in the saturator. By changing the ratio of the two He streams, the different activity (the ratio of vapor partial pressure to saturation pressure) of adsorbates could be achieved.

2.5. Molecular dynamic simulations

2.5.1. Potential models and system set up

The framework of Sodium Mordenite (MOR) zeolite was generated from a unit cell from the database IZA-SC by repeating the unit cell 2 × 2 × 3 on a, b and c respectively. Since we are concerned with the structural properties like expansion or contraction, three-dimensional periodic condition was not appropriate in our case. We discussed in detail in our previous paper [28], so in this study we introduced a

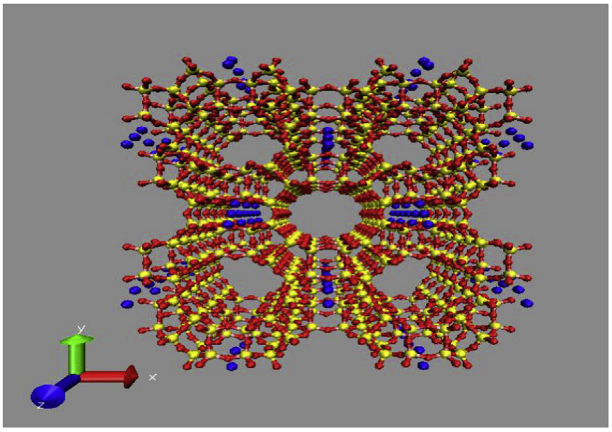

Fig. 1. Perspective view of MOR frameworks (Yellow: Si/Al; Red: O; Blue: Na). (For interpretation of the references to colour in this figure legend, the reader is referred to the Web version of this article.)

Table 1
Simulation parameters for models used.

Molecule	Element	σ (Å)	ε (kcal/mole)	q (e)
MOR zeolite	Si	2.970	0.0635	1.0720
	Al	3.140	0.0477	1.4130
	O	3.011	0.1063	−0.7476
	Na	3.230	0.4652	1.0000
Water(TIP3P)	O	3.151	0.1521	−0.8340
	H	0.400	0.0460	0.4170

system with two periodic boundaries in the X and Y direction and left empty spaces (vacuum) on both side of the crystal structure in Z direction as shown in Fig. 1 to allow for expansion/contraction. The potential parameters are taken from B. Vujić et al. [29] shown in Table 1, which were used to simulate the behavior of non-polar gases in the zeolite frameworks. We used our previous method [14,30] to examine if the zeolite structure expands or shrinks. The framework atoms are tethered to their perfect crystal sites with a suitable strength harmonic constant to allow for structural flexibility in the model. The potential model for water molecules is the TIP3P model [31] implemented and slightly modified in CHARMM [32]. The potential energy in the system can be described by the following equation:

$$E_{total} = \sum_{bonds} K_b(b - b_{eq})^2 + \sum_{angles} K_\theta(\theta - \theta_{eq})^2 + \sum_{i<j} \left\{ 4\varepsilon \left[\left(\frac{\sigma_{ij}}{r_{ij}} \right)^{12} - \left(\frac{\sigma_{ij}}{r_{ij}} \right)^{6} \right] + \frac{q_i q_j}{4\varepsilon_0 r_{ij}} \right\} \quad (3)$$

There are both intramolecular and intermolecular contributions in the potential model. The flexible bond lengths and bond angles are represented by the first two terms, while intermolecular contribution was described by the third term using Lenard-Jones 12-6 potentials and classic coulombic interactions. Both LJ and coulombic forces were cut off by 14 Å.

2.5.2. Details of simulation

The simulations were performed in term of non-equilibrium conditions with the LAMMPS simulation package and the time integration was carried out by the verlet algorithm [33]. It kept the system volume constant. A constant temperature of 100 °C was maintained by applying a Nosé-Hoover thermostat (with a damping constant of 1 fs) to the solution and membrane atoms throughout the simulation. A time step of 0.01 fs was used for production runs of 100 million steps (1 ns). The number of water molecules absorbed is measured by counting the number inside the crystal region. The contraction/expansion percentage is measured by comparing the distances between two surfaces' in the Z direction. All results were generated by running averages of every 500 thousand-time steps of the last 40 million time steps to ensure that we were approaching equilibria.

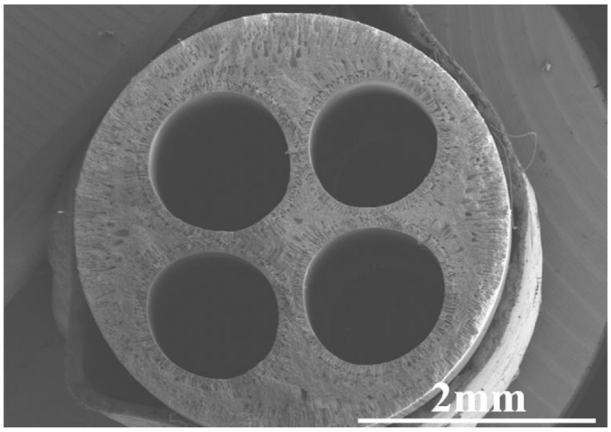

Fig. 2. Cross-section SEM image of four-channel α-Al_2O_3 hollow fiber support.

3. Results and discussion

3.1. Characterization of mordenite seeds and seeding layers

Fig. 2 displays the SEM images of the cross-section of four-channel α-Al_2O_3 hollow fiber support. A large amount of finger-like pores which resulted in the low mass resistance and the improvement of the flux of mordenite zeolite membranes would be observed. Fig. 3a–c shows the SEM images of the original mordenite crystals and zeolite seeds after different ball-milled treatment time. The original zeolite particles with disk-like shape having a particle size about 4 μm could be observed in Fig. 3a. After 1 h ball milling, most mordenite seeds cracked to some small pieces (Fig. 3b), while some unbroken mordenite particles were also observed, as marked with red circles. With the ball milling time increasing to 3 h, homogeneous mordenite particles average size of about 300 nm could be obtained (Fig. 3c), which was confirmed by the result of particle size analyzer. Compared with original mordenite particles, the surface of ball-milled seeds may expose more nucleation sites which are beneficial for quick crystallization [34] to fabricate defect-free zeolite membrane. Meanwhile, the decreasing of particle size could improve stability of seed suspension helping the preparation of continuous seed layer. XRD patterns as shown in Fig. 4 confirmed that the obtained particles with mordenite structure. With the extension of ball milling time, the intensity of mordenite phase peak decreased which might be due to the chemical bond rupture of Si—O—Si and Si—O—Al in the molecular sieves [35]. When using the original mordenite zeolite as seeds to form the seed layer, the hollow fiber support could not be completely covered (Fig. 3d), which significantly increased the defects number in the zeolite membranes [36]. A mordenite seed layer of considerable uniformity and continuity could be obtained by using ball-milled particles, as shown in Fig. 3e and f.

3.2. Characterization of mordenite zeolite membranes

The XRD patterns of as-synthesized zeolite membranes induced with ball-milled seeds for different treatment time were revealed by Fig. 5. It was noted that all of membranes had typical mordenite and α-Al_2O_3 support diffraction peaks. Fig. 6a–f shows the surface and cross-section SEM images of as-fabricated mordenite zeolite membranes. With the zeolite seeds size decreasing, both the size of crystals composing the membrane and the membrane thickness decreased. The reason could be that ball-milled particles possessed more nucleation sites due to lattice

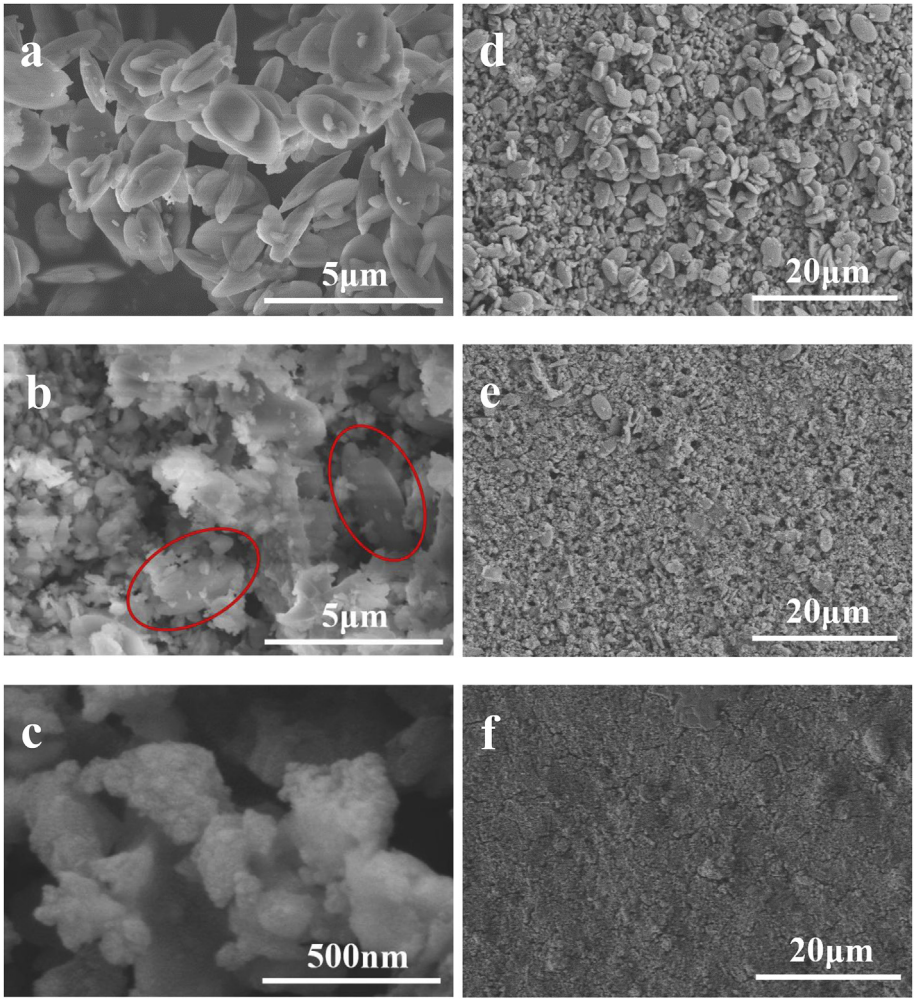

Fig. 3. SEM images of mordenite seeds and seed layers for original (a, d), 1 h ball milling (b, e) and 3 h ball milling (c, f).

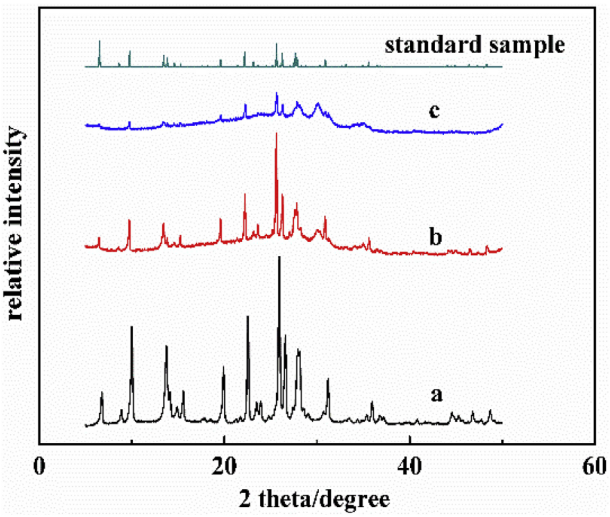

Fig. 4. XRD patterns of mordenite seeds of original (a) and ball milling time of 1 h (b), 3 h (c).

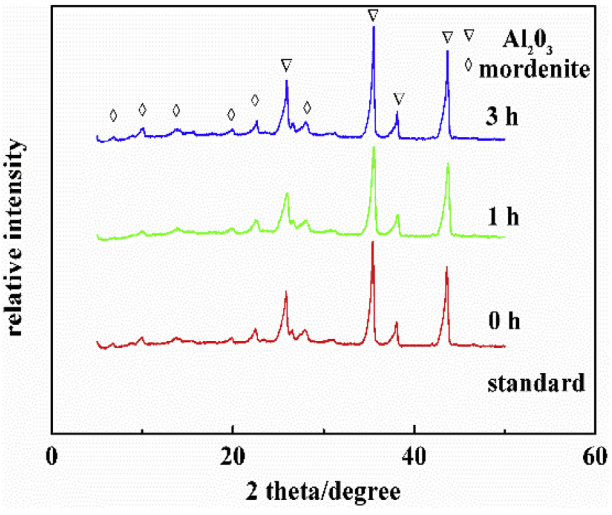

Fig. 5. XRD patterns of mordenite membranes induced with original particles (a) and ball-milled seeds with treatment time of 1 h (b), 3 h (c).

defects promoting the nucleating of zeolite [26]. Compared with the membrane prepared from original seeds, the surface of membrane prepared from ball milling seeds were more even, and no obvious intercrystalline gaps existed.

3.3. PV and VP performance for IPA/water mixture dehydration

3.3.1. Effect of mordenite particle size

The separation data on pervaporation performance for IPA/H_2O (90/10 wt%) mixture separation at 75 °C of the zeolite membrane

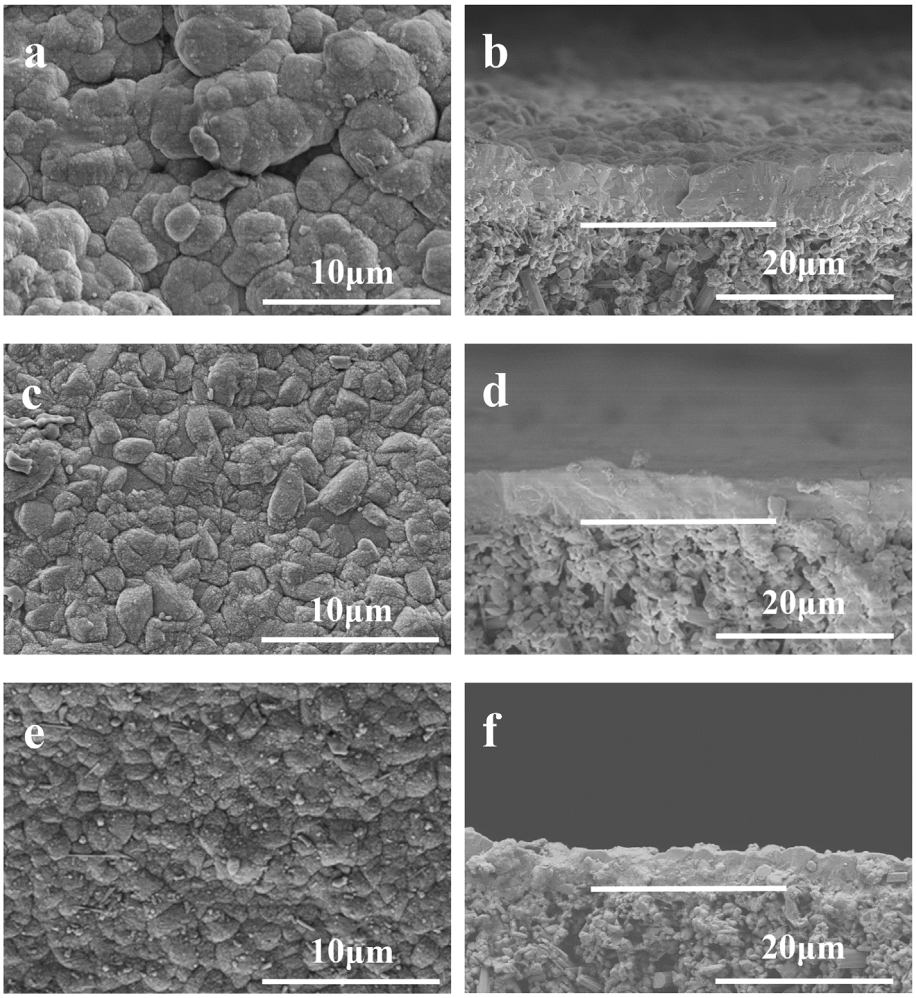

Fig. 6. SEM images of mordenite zeolite membranes induced with original particles (a and b) and ball-milled seeds with treatment time of 1 h (c and d), 3 h (e and f).

Table 2
Effect of the seed size on the performance of as-synthesized mordenite zeolite membranes for IPA/H_2O (90/10 wt%) mixture dehydration at 75 °C.

Membrane sample	Seed size (μm)	Membrane thickness (μm)	Q ($kg \cdot m^{-2} \cdot h^{-1}$)	$\alpha_{water/IPA}$
M-01	~4	~12	4.35	5
M-02	~1	~10	1.05	605
M-03		~9	0.98	572
M-04	~0.3	~7	1.40	4374
M-05		~6	1.50	5143
M-06		~8	1.45	6963
M-07		~7	1.43	> 10000

prepared with different sizes of seed is shown in Table 2. It was found that the mordenite membrane (M-01) induced by using original seeds presented low performance with only a separation factor of 5 for IPA over H_2O. The existence of intercrystalline gaps observed in its SEM image is the most likely reason. The synthesized membranes of M-04, M-05, M-06, M-07 induced with ball-milled seeds for treatment time of 3 h showed high separation factors that were up to 4374, 5143, 6963, > 10000, respectively. And these were attributed to their well-intergrown zeolite layers in Fig. 6e. Meanwhile, their permeation fluxes were all above 1.40 $kg\,m^{-2}\,h^{-1}$ because of their thinner thickness of membranes, which were all about 7 μm. The data shown in Table 2 was found to be consistent with the SEM images (Fig. 6). Therefore, the membranes prepared by using ball-milled seeds showed fewer defects, resulted in much smaller zeolite crystals on the top of membranes and thinner thickness which led to higher separation factors and permeation flux for dehydration of IPA/water mixture at the same time. So, it is evident that ball-milled seeds should be employed for fabricating mordenite zeolite membranes. In addition, as shown in Table 3, the performance of mordenite zeolite membranes prepared by using ball-milled seeds with 3 h treatment time for different organic solution at 75 °C is significantly improved. The comparison of pervaporation performance of mordenite membranes prepared by different work is reported in Table 4. The mordenite membranes prepared by using ball-milled seeds with treatment time for 3 h (M-07) showed good separation performance with a high permeation flux of 1.43 $kg\,m^{-2}\,h^{-1}$ and selectivity of > 10000 at 75 °C. Although the membranes prepared by microwave synthesis also show good performance, the method might be too complex for industrial application.

Table 3
Pervaporation performance of mordenite zeolite membrane (M-06) for different organic mixtures dehydration at 75 °C.

Feed mixture composition	Q ($kg \cdot m^{-2} \cdot h^{-1}$)	$\alpha_{water/organic}$
90 wt% EtOH/H_2O	1.01	4684
70 wt% EtOH/H_2O	1.22	> 10000
90 wt% IPA/H_2O	1.45	6963
70 wt% IPA/H_2O	2.10	> 10000
90 wt% HAc/H_2O	0.47	2150

Table 4
The dehydration performance of mordenite zeolite membranes for IPA/H_2O (90/10 wt%) mixtures reported in the literature and in this work.

Support	Synthetic method	Operating temperature (°C)	Q (kg·m^{-2}·h^{-1})	Separation factor	References
α-Al_2O_3 tube	In situ	75	0.10	3360	[21]
α-Al_2O_3 tube	Secondary growth	75	0.65	5000	[17]
Mullite tube	Secondary growth	75	1.85	3300	[23]
α-Al_2O_3 tube	Secondary growth (micro-assisted)	75	1.40	> 10000	[24]
α-Al_2O_3 hollow fiber	Secondary growth	75	1.43	> 10000	This work
		100(VP)	2.66	> 10000	

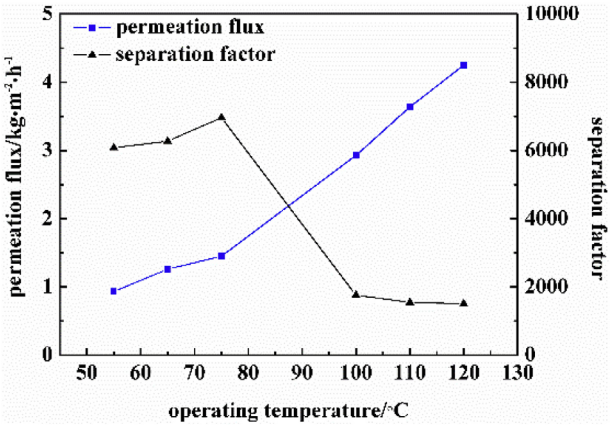

Fig. 7. Influence of operating temperature on dehydration performance of as-synthesized mordenite zeolite membrane (M-06) for IPA/H_2O (90/10 wt%) mixture dehydration.

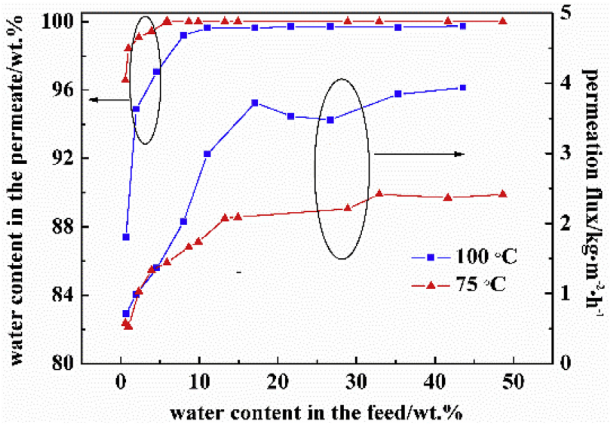

Fig. 8. The PV at 75 °C and VP at 100 °C results of mordenite zeolite membrane (M-06) for IPA/H_2O mixture dehydration at different feed water content.

3.3.2. Effect of operating temperature

Mordenite zeolite membranes prepared by using ball-milled seeds for 3 h treatment time were used to study the effect of operating parameters, such as feed temperature and feed water contention the separation performance. Fig. 7 reveals the influence of operating temperature in range from 55 to 75 °C (PV) and 100–130 °C (VP) on IPA/H_2O (90/10 wt%) mixture dehydration performance of M-06. The flux of mordenite membrane increased from 0.93 kg m^{-2} h^{-1} to 1.45 kg m^{-2} h^{-1} when the operating temperature increased 55 °C–75 °C. Meanwhile, the separation factors maintained a high level of > 6000. Raising the operating temperature from 100 °C to 130 °C (operated by vapor permeation) doubled the permeation flux. This could have been expected since the IPA/H_2O liquid mixture was transformed into gas mixture, and there was extremely low impact of concentration polarization on membrane surface in vapor permeation. However, the separation factor decreased from 6963 to 1758 because IPA molecules diffusivity were accelerated by water molecules that have higher diffusivity [37]. Mordenite membranes showed relatively lower flux compared with NaA membranes in similar separation system [38]. The relatively high hydrophilicity of NaA originating from its low Si/Al ratio (~1) might be the reason.

3.3.3. Effect of feed water content

Fig. 8 shows the influence of water content in feed side ranging from 0.5 wt% to 50 wt% on the water content in the permeate and flux of mordenite zeolite membrane (M-06) at 75 °C (PV) and 100 °C (VP). With the increasing feed water content, the permeation fluxes at both temperature increased gradually from 0.5 wt% to 30 wt%. This is a typical phenomenon when an adsorption–diffusion mechanism dominates the membrane separation performance [39]. Within the tested range of water content, a relative high water content in the permeate could be obtained for pervaporation at 75 °C than that for vapor permeation at 100 °C, especially when the feed water content was below 5 wt%. At low feed water content, water concentration in the permeate was only about 87.4% at 100 °C by vapor permeation because the isopropanol molecules occupied adsorption sites more easily than water molecules in zeolite pores and nonzeolite pores [40].

3.4. The stability of mordenite membrane in vapor permeation

3.4.1. VP results of MOR zeolite membranes for binary mixture separation

Previous studies have revealed that the NaA membrane dehydration performance for H_2O/alcohol (methanol (MeOH), EtOH and IPA) mixtures depends on molecular size of alcohol when the feed water content is low. NaA membranes show relatively poor performance for IPA/H_2O mixture separation at low feed water content because of the shrinkage of NaA zeolite crystals leading to large defects [14]. Mordenite zeolite membrane were therefore used to study H_2O/alcohol (MeOH, EtOH and IPA) mixtures dehydration performance with water content ranging from 0.5 wt% to 10 wt% in detail. As shown in Fig. 9, the membrane maintained water content (> 99 wt%) in the permeate

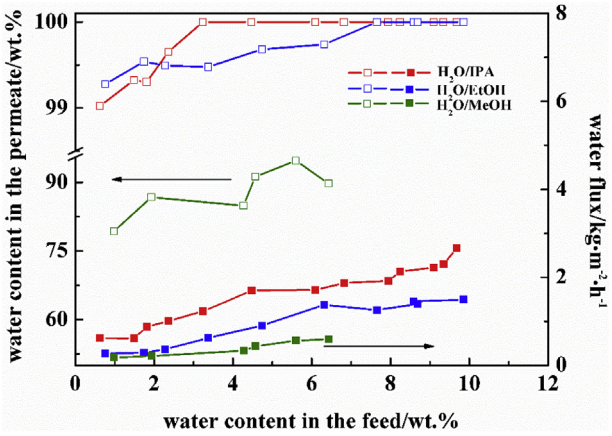

Fig. 9. The VP results at 100 °C of mordenite zeolite membrane (M-07) for H_2O/alcohol (MeOH, EtOH and IPA) mixtures dehydration at different feed water content.

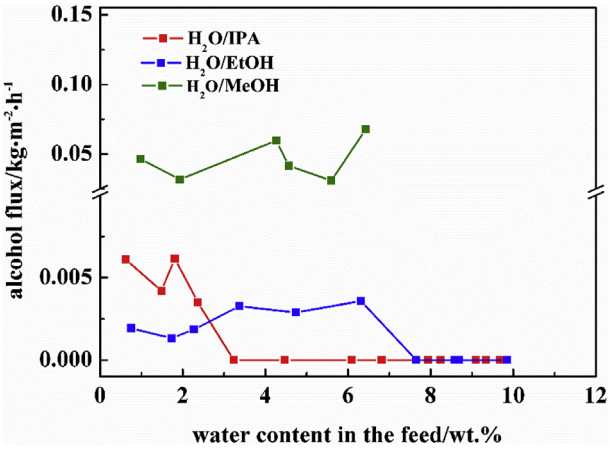

Fig. 10. The VP results for alcohol flux at 100 °C of mordenite zeolite membrane (M-07) for H_2O/alcohol mixtures dehydration at different feed water content.

at low water content in the feed for both EtOH/H_2O and IPA/H_2O mixtures, and its selectivity was always above 10000. The separation factor was only about 300 for methanol/water mixture because the dynamic diameter of methanol is much smaller than the mordenite pore diameter. The flux of membrane in above systems decreased with the feed water content as a result of the lower driving force. Fig. 10 demonstrates that ethanol and IPA flux were all below 0.007 kg m^{-2} h^{-1} at feed water content below 5 wt%. It should be noticed that the mordenite membrane maintained almost 100 wt% water content in the permeate for 97 wt% IPA/water mixture. This result shows that the mordenite zeolite membrane is quite stable at lower water content, and the shrinkage of mordenite crystal framework also did not occur.

To understand the stability of mordenite zeolitic structure, we studied the adsorption characteristics of mordenite membrane by permporosimetry measurements. The change of the helium (He) permeance of membrane was investigated when the mordenite membrane adsorbed H_2O, MeOH, EtOH and IPA at different activities, as shown in Fig. 11. When the activity was below 0.3, the He permeance drastically decreased with increasing activity for all adsorbates. The micropores of zeolite were blocked, because the pore size of mordenite zeolites is larger than the dynamic diameter of all of adsorbates. Further increasing the activity, the He permeance decreased and approached to zero, which implied that both membrane defects and zeolitic pores had been closed at these conditions. In the case of water as adsorbate, the He permeance decreased the most because the dynamic diameter of

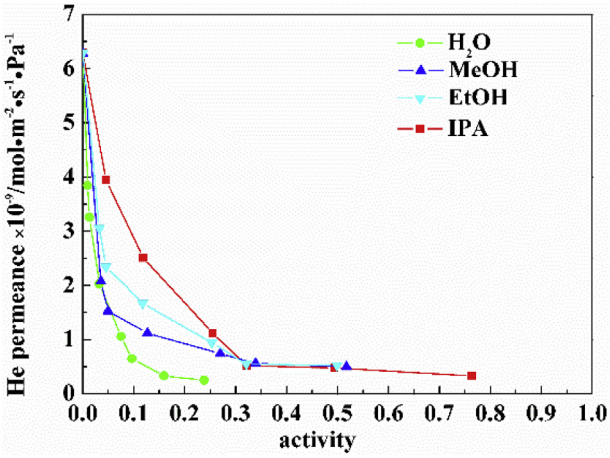

Fig. 11. He permeance of mordenite zeolite membrane at 40 °C as a function of H_2O, MeOH, EtOH and IPA activity under pressure drop of 0.1 MPa.

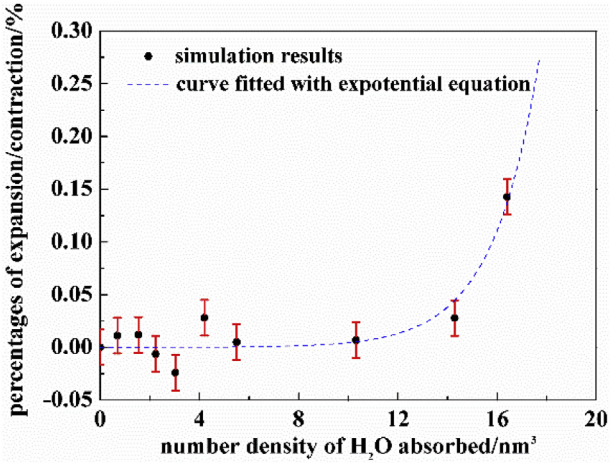

Fig. 12. The influence of number density of water loading on size changes of zeolite framework. (Number densities are evaluated by the pore volume, which is 50% of the total unit cell volume [42]).

water is the smallest. The phenomenon observed in mordenite membranes was quite different from that in NaA membrane during permporosimetry measurements. In the case of NaA zeolite membrane, the helium permeance increased first and then decreased rapidly with increasing of water activity because the shrinkage of NaA zeolite led to the expansion of membrane defects [14]. Combining the results of vapor permeation experiment and permporosimetry measurement, we could conclude that the structure of mordenite crystals did not change after solvent absorption which we attribute to the relatively high Si/Al ratio.

3.4.2. Effect of adsorbate water on expansion/contraction of mordenite crystal framework

The results of molecular simulation is demonstrated in Fig. 12, which shows that MOR zeolite framework is relative rigidity at low water loadings, but with the increasing of the amounts of loading water, the zeolite framework has a tendency to expand. When the amount of loading water is low, it inclines to accumulate in the zeolite cavity center before accumulating on the framework sites. This dynamic is due to the strongly polar nature of the water molecules being attracted towards the center. In addition, water molecules also accumulate in the smaller cavities and the two effects essentially cancel out with some oscillatory behavior observed. This is somewhat different than the trends in our previous work of LTA zeolite frameworks which does not have the smaller cavities present in MOR [14]. With the increasing of amount of the loading water, they start to occupy the framework atoms nearby areas, and repulsive forces then tend to push the framework molecules out, leading to the zeolite framework expansion. This expansion is also observed by others in their simulation works [41] and can demonstrate the correctness of the potential model and simulation work. The error bars were obtained by doubling the length of the simulations in selected cases, as well as starting the simulations with different initial configurations.

3.4.3. Stability test of MOR membrane under water rich condition

Previous study showed that, the structure of LTA type membrane [16] could be destroyed leading to poor performance under water rich condition because of its low Si/Al ratio. Mordenite, with a higher Si/Al ratio, is expected to be more stable. We tested the stability performance of mordenite membrane for dehydration of IPA/H_2O (50/50 wt%) mixture at 100 °C for 120 h by vapor permeation and Fig. 13 shows the results. The permeation flux and the permeate water content was about 4 kg m^{-2} h^{-1} and 100 wt%, respectively. These results confirm the stability of mordenite zeolite membrane for high feed water content

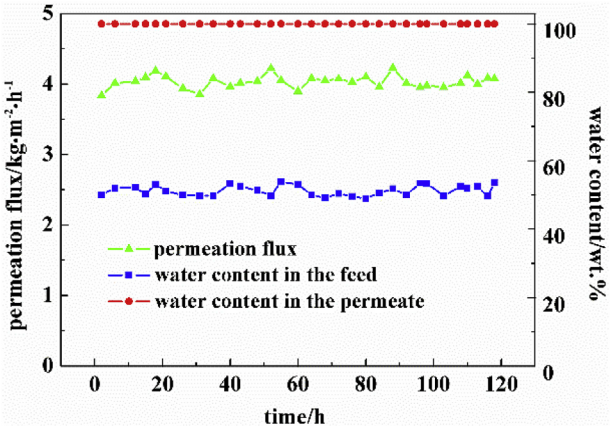

Fig. 13. The VP results of mordenite zeolite membrane (M-07) for IPA/H_2O (50/50 wt%) dehydration during a long time test at 100 °C.

dehydration systems.

4. Conclusions

Overall, the four-channel α-Al_2O_3 hollow fiber supported mordenite zeolite membranes induced by the ball-milled seed layers showed high pervaporation performance for IPA/H_2O mixture dehydration. The mordenite membrane induced with seeds ball-milled for 3 h exhibited a high selectivity of beyond 10000 and the permeation flux of 1.43 kg m^{-2} h^{-1} at 75 °C for IPA/H_2O (90/10 wt%) mixture. The mordenite membrane synthesized showed high performance for feed water concentration between 0.5 and 10 wt% and long time stability at high water concentration of 50 wt% in the feed for 120 h at 100 °C. Permporosimetry studies and molecular simulation showed that the framework of MOR zeolite was relatively rigid compared to that of NaA, and both MOR zeolite crystal unit cell size and the size of defects in the zeolite membrane were less affected by water adsorption. That is responsible in part for the stable performance for MOR zeolite membrane at low feed water content. Meanwhile the structure stability of zeolite membrane at high water content is also improved due to the high Si/Al ratio of framework of MOR. Our research has shown that, mordenite zeolite membranes are promising membrane materials for vapor phase dehydration of alcohols in the industrial application.

Acknowledgements

This research was supported by the National Natural Science Foundation of China (21490585 and 21606126), National High-tech R &D Program of China (2015AA03A602), “333 Talent Project” of Jiangsu Province and State Key Laboratory of Materials-Oriented Chemical Engineering (No. ZK201719). XW and SM were also sponsored by a grant from the US National Science Foundation (CBET 1545560).

References

[1] X. Feng, R. Huang, Liquid separation by membrane pervaporation: a review, Ind. Eng. Chem. Res. 36 (1997) 1048–1066.
[2] A. Alomair, S. Al-Jubouri, S. Holmes, A novel approach to fabricate zeolite membranes for pervaporation processes, J. Mater. Chem. A. 3 (2015) 9799–9806.
[3] J. Caro, M. Noack, P. Kölsch, R. Schäfer, Zeolite membranes-state of their development and perspective, Microporous Mesoporous Mater. 38 (2000) 3–24.
[4] T. Bowen, R. Noble, J. Falconer, Fundamentals and applications of pervaporation through zeolite membranes, J. Membr. Sci. 245 (2004) 1–33.
[5] J. Jiang, L. Wang, L. Peng, C. Cai, C. Zhang, X. Wang, X. Gu, Preparation and characterization of high performance CHA zeolite membranes from clear solution, J. Membr. Sci. 527 (2017) 51–59.
[6] F. Zhang, Y. Zheng, L. Hu, N. Hu, M. Zhu, R. Zhou, X. Chen, H. Kita, Preparation of high-flux zeolite T membranes using reusable macroporous stainless steel supports in fluoride media, J. Membr. Sci. 456 (2014) 107–116.
[7] X. Wang, Y. Chen, C. Zhang, X. Gu, N. Xu, Preparation and characterization of high-flux T-type zeolite membranes supported on YSZ hollow fibers, J. Membr. Sci. 455 (2014) 294–304.
[8] S. Basak, D. Kundu, M. Naskar, Low temperature synthesis of NaA zeolite membranes: the effect of primary and secondary crystallizations, Ceram. Int. 40 (2014) 12923–12930.
[9] X. Shu, X. Wang, Q. Kong, X. Gu, N. Xu, High-flux MFI zeolite membrane supported on YSZ hollow fiber for separation of ethanol/water, Ind. Eng. Chem. Res. 51 (2012) 12073–12080.
[10] D. Kunnakorn, T. Rirksomboon, P. Aungkavattana, N. Kuanchertchoo, D. Atong, K. Hemra, S. Kulprathipanja, S. Wongkasemjit, Optimization of synthesis time for high performance of NaA zeolite membranes synthesized via autoclave for water-ethanol separation, Desalination 280 (2011) 259–265.
[11] V. Sebastian, R. Mallada, J. Coronas, A. Julbe, R.A. Terpstra, R.W.J. Dirrix, Microwave-assisted hydrothermal rapid synthesis of capillary MFI-type zeolite–-ceramic membranes for pervaporation application, J. Membr. Sci. 355 (2010) 28–35.
[12] Y. Morigami, M. Kondo, J. Abe, H. Kita, K. Okamoto, The first large-scale pervaporation plant using tubular-type module with zeolite NaA membrane, Separ. Purif. Technol. 25 (2001) 251–260.
[13] C. Yu, Y. Liu, G. Chen, X. Gu, W. Xing, Pretreatment of isopropanol solution from pharmaceutical industry and pervaporation dehydration by NaA zeolite membranes, Chin. J. Chem. Eng. 19 (2011) 904–910.
[14] F. Qu, R. Shi, L. Peng, Y. Zhang, X. Gu, X. Wang, S. Murad, Understanding the effect of zeolite crystal expansion/contraction on separation performance of NaA zeolite membrane: a combined experimental and molecular simulation study, J. Membr. Sci. 539 (2017) 14–23.
[15] S. Sorenson, E. Payzant, W. Gibbons, B. Soydas, H. Kita, R.D. Noble, J.L. Falconer, Influence of zeolite crystal expansion/contraction on NaA zeolite membrane separations, J. Membr. Sci. 366 (2011) 413–420.
[16] K. Sawamura, T. Furuhata, Y. Sekine, E. Kikuchi, B. Subramanian, M. Matsukata, Zeolite membrane for dehydration of isopropylalcohol-water mixture by vapor permeation, ACS Appl. Mater. Interfaces 7 (2015) 13728–13730.
[17] G. Li, E. Kikuchi, M. Matsukata, Separation of water-acetic acid mixtures by pervaporation using a thin mordenite membrane, Separ. Purif. Technol. 32 (2003) 199–206.
[18] X. Li, H. Kita, H. Zhu, Z. Zhang, K. Tanaka, Synthesis of long-term acid-stable zeolite membranes and their potential application to esterification reactions, J. Membr. Sci. 339 (2009) 224–232.
[19] L. Li, J. Yang, J. Li, P. Han, J. Wang, Y. Zhao, J. Wang, J. Lu, D. Yin, Y. Zhang, Synthesis of high performance mordenite membranes from fluoride-containing dilute solution under microwave-assisted heating, J. Membr. Sci. 512 (2016) 83–92.
[20] M. Zhu, X. Hua, Y. Liu, H. Hu, Y. Li, N. Hu, I. Kumakiri, X. Chen, H. Kita, Influences of synthesis parameters on preparation of acid-stable and reproducible mordenite membrane, Microporous Mesoporous Mater. 55 (2016) 12268–12275.
[21] X. Lin, E. Kikuchi, M. Matsukata, Preparation of mordenite membranes on α-alumina tubular supports for pervaporation of water-isopropyl alcohol mixtures, Chem. Commun. (2000) 957–958.
[22] A. Navajas, R. Mallada, C. Téllez, J. Coronas, M. Menéndez, J. Santamaría, The use of post-synthetic treatments to improve the pervaporation performance of mordenite membranes, J. Membr. Sci. 270 (2006) 32–41.
[23] R. Zhou, Z. Hu, N. Hu, L. Duan, X. Chen, H. Kita, Preparation and microstructural analysis of high-performance mordenite membranes in fluoride media, Microporous Mesoporous Mater. 156 (2012) 166–170.
[24] M. Zhu, S. Xia, X. Hua, Z. Feng, N. Hu, F. Zhang, I. Kumakiri, Z. Lu, X. Chen, H. Kita, Rapid preparation of acid-stable and high dehydration performance mordenite membranes, Ind. Eng. Chem. Res. 53 (2014) 19168–19174.
[25] D. Liu, Y. Zhang, J. Jiang, X. Wang, C. Zhang, X. Gu, High-performance NaA zeolite membranes supported on four-channel ceramic hollow fibers for ethanol dehydration, RSC Adv. 5 (2015) 95866–95871.
[26] Z. Yang, Y. Liu, C. Yu, X. Gu, N. Xu, Ball-milled NaA zeolite seeds with submicron size for growth of NaA zeolite membranes, J. Membr. Sci. 392–393 (2012) 18–28.
[27] H. Zhou, C. Zhang, X. Gu, W. Jin, N. Xu, A simple method for healing nonzeolitic pores of MFI membranes by hydrolysis of silanes, J. Membr. Sci. 366 (2011) 427–435.
[28] X. Wang, X. Gu, S. Murad, Molecular dynamics simulations of liquid-liquid phase equilibrium of ternary methanol/water/hydrocarbon mixtures, Fluid Phase Equil. (2017) 1–11.
[29] B. Vujić, A.P. Lyubartsev, Transferable force-field for modelling of CO_2, N_2, O_2 and Ar in all silica and Na^+ exchanged zeolites, Model. Simul. Mater. Sc. 24 (2016) 045002.
[30] S. Murad, P. Ravi, J. Powles, A computer simulation study of fluids in model slit, tubular, and cubic micropores, J. Chem. Phys. 98 (1993) 9771–9781.
[31] W. Jorgensen, J. Chandrasekhar, J. Madura, R. Impey, M.L. Klein, Comparison of simple potential functions for simulating liquid water, J. Chem. Phys. 79 (1983) 926–935.
[32] A. MacKerell Jr., D. Bashford, M. Bellott, R. Dunbrack Jr., J. Evanseck, M. Field, S. Fischer, J. Gao, H. Guo, S. Ha, All-atom empirical potential for molecular modeling and dynamics studies of proteins, J. Phys. Chem. B 102 (1998) 3586–3616.
[33] S. Plimpton, Fast parallel algorithms for short-range molecular dynamics, J. Comput. Phys. 117 (1995) 1–19.
[34] V. Valtchev, S. Mintova, V. Dimov, A. Toneva, D. Radev, Tribochemical activation of seeds for rapid crystallization of zeolite Y, Zeolites 15 (1995) 193–197.
[35] C. Kosanović, J. Bronić, A. Čižmek, B. Subotić, I. Šmit, M. Stubičar, A. Tonejc, Mechanochemistry of zeolites: Part 2. Change in particulate properties of zeolites during ball milling, Zeolites 15 (1995) 247–252.

[36] X. Zhang, H. Liu, K. Yeung, Influence of seed size on the formation and microstructure of zeolite silicalite-1 membranes by seeded growth, Mater. Chem. Phys. 96 (2006) 42–50.
[37] M. Yu, J. Falconer, R. Noble, R. Krishna, Modeling transient permeation of polar organic mixtures through a MFI zeolite membrane using the Maxwell-Stefan equations, J. Membr. Sci. 293 (2007) 167–173.
[38] M. Kondo, T. Yamamura, T. Yukitake, Y. Matsuo, H. Kita, K. Okamoto, IPA purification for lens cleaning by vapor permeation using zeolite membrane, Separ. Purif. Technol. 32 (2003) 191–198.
[39] Y. Liu, Z. Yang, C. Yu, X. Gu, N. Xu, Effect of seeding methods on growth of NaA zeolite membranes, Microporous Mesoporous Mater. 143 (2011) 348–356.
[40] X. Wang, Y. Chen, C. Zhang, X. Gu, N. Xu, Preparation and characterization of high-flux T-type zeolite membranes supported on YSZ hollow fibers, J. Membr. Sci. 455 (2014) 294–304.
[41] G. Maurin, R. Bell, S. Devautour, F. Henn, J. Giuntini, Modeling the effect of hydration in zeolite Na mordenite, J. Phys. Chem. B 108 (2004) 3739–3745.
[42] E. First, C. Gounaris, J. Wei, C. Floudas, Computational characterization of zeolite porous networks: an automated approach, Phys. Chem. Chem. Phys. 13 (2011) 17339–17358.